Turning angle control of power kites for wind energy

Conference Paper *in* Proceedings of the IEEE Conference on Decision and Control · December 2013

DOI: 10.1109/CDC.2013.6760419

3 authors:

Ramiro Saraiva
Serviço Nacional de Aprendizagem Industrial
10 PUBLICATIONS **232** CITATIONS
SEE PROFILE

Marcelo De Lellis Costa de Oliveira
Universidade Federal de Santa Catarina
15 PUBLICATIONS **291** CITATIONS
SEE PROFILE

A. Trofino
Universidade Federal de Santa Catarina
153 PUBLICATIONS **3,859** CITATIONS
SEE PROFILE

52nd IEEE Conference on Decision and Control
December 10-13, 2013. Florence, Italy

Turning Angle Control of Power Kites for Wind Energy

Marcelo De Lellis, Ramiro Saraiva and Alexandre Trofino

Abstract— **In this paper, we model and identify the turning angle dynamics of a power kite and propose a control scheme with two loops. The outer loop uses Bernoulli's lemniscate as an offline-optimized trajectory to generate a reference for the inner loop, which controls the turning angle through feedback linearization. We present simulation results of electric power generation and control performance, also under wind turbulence.**

I. INTRODUCTION

Energy is a fundamental resource for the development of nations and social welfare. It is expected that the world's energy demand will increase more than one third by the year 2035 [1]. Despite recent developments in energy sources with low carbon emissions, fossil fuels remain dominant in the energy mix, but bring on a handful of environmental and political problems. In response to these issues there is a need for further development and deployment of renewable energy technologies, such as those based on wind.

In the last decade, power kites emerged as an alternative to the wind turbines. The advantages of this new approach can be better exploited by optimally determining some parameters as tether length, (un)winding speed, and orbit characteristics. Several configurations of such systems based on tethered airfoils have been proposed [2], and a mix of off and online optimization has been used for power maximization, combined with either open or closed orbits[1].

The problem of designing the optimal reference for closed orbits was investigated in [3], whereas in [4] such reference orbits were tracked through a mixed NMPC and linear state feedback control scheme, aided by state estimation. NMPC was also employed in [5], where the tracking problem was addressed jointly with the optimal open orbit reference design, while in [6] a closed orbit was determined offline and tracked with an MPC inner loop. However, more recently [7] established a higher energy efficiency of open over closed orbits. Finally, [8], [9] solved the tracking problem by introducing the *turning angle* variable, which represents the kite's velocity vector direction and allows a decoupling between trajectory reference generation and the kite dynamics. A similar approach was used by [10], however with a constant tether length, to control a towing kite for seagoing vessels.

This work was financially supported by CAPES, Brazil.

M. De Lellis C. de Oliveira (PhD student), R. Saraiva da Silva (MSc student) and A. Trofino are with the Department of Automation and Systems Engineering, Federal University of Santa Catarina, DAS/CTC/UFSC, Florianpolis, SC, Brazil. E-mails: [lellis,ramiro,trofino]@das.ufsc.br

[1]A single closed orbit comprises both reel-out (traction) and reel-in (passive) phases, whereas each phase can also be made of one or more open orbits.

This paper exploits the turning angle concept and focuses on three main contributions:

- Use of Bernoulli's lemniscate as an optimal trajectory approximation for power maximization in the traction phase using open orbits;
- Proposal of an alternative characterization of the turning angle dynamics and discussion of the identification of the model parameters;
- Control of the turning angle by means of *feedback linearization* in order to track a trajectory reference.

The rest of the paper is organized as follows: section II approaches the kite model based on which the turning angle dynamics is then modeled and identified. The control design and tuning is presented in section III. The system parameters are optimally chosen in section IV and the simulation results of power generation and control performance are discussed in section V. Section VI concludes the paper.

Notation: $\|\mathbf{v}\|$ is the euclidean norm of a vector $\mathbf{v}$, its transpose is $\mathbf{v}^T$, and its representation in the inertial, local, and lemniscate frames is $(\cdot)_i$, $(\cdot)_l$, and $(\cdot)_L$, respectively. The inner and cross product of two vectors are $\mathbf{v}_1 \bullet \mathbf{v}_2$ and $\mathbf{v}_1 \times \mathbf{v}_2$, whereas $|u|$, $\overline{u}$, $\underline{u}$, $\sigma(u)$, and $\tilde{u}$ represent the magnitude, maximum, minimum, standard deviation and average values of a scalar u. Vectors and scalars are continuous-time variables, if not otherwise stated. $\dot{(\cdot)}$, $\ddot{(\cdot)}$ are their 1st and 2nd time-derivatives.

II. SYSTEM MODEL

We use a point-mass approximation of the airfoil tethered to a fixed point on the ground by means of two cables of length r_a, defining a spherical flight surface. The nominal wind is $\mathbf{W_n} = \big(W_x(z_a), 0, 0\big)_i$, and the so-called *wind window* is limited to the upper-half downwind fourth of the sphere, as illustrated in Fig. 1. The airfoil position vector is $\mathbf{r_a} = r_a(\sin\theta_a \cos\phi_a, \sin\theta_a \sin\phi_a, \cos\theta_a)_i$, and the local frame is defined by the vectors $\mathbf{e}_\theta = d\mathbf{r_a}/d\theta_a$, $\mathbf{e}_\phi = d\mathbf{r_a}/d\phi_a$ and $\mathbf{e_r} = \mathbf{e}_\theta \times \mathbf{e}_\phi$.

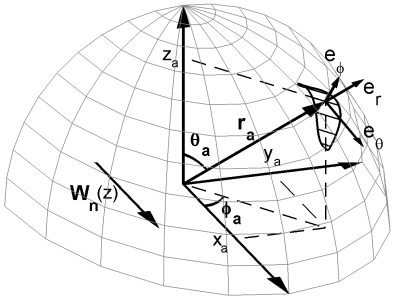

Fig. 1: Kite wind window, inertial $(\mathbf{x}, \mathbf{y}, \mathbf{z})_i$, and local $(\mathbf{e}_\theta, \mathbf{e}_\phi, \mathbf{e_r})_l$ frames.

Flight dynamics is determined by gravity, apparent (inertial and Coriolis), aerodynamic and cable traction forces, evaluated in the local frame, as

$$m \begin{bmatrix} r_a\ddot{\theta}_a \\ r_a\ddot{\phi}_a \sin\theta_a \\ \ddot{r}_a \end{bmatrix}_l = \mathbf{F}^{\text{grav}} + \mathbf{F}^{\text{app}} + \mathbf{F}^{\text{aer}} - \begin{bmatrix} 0 \\ 0 \\ F_r^{\text{trac}} \end{bmatrix}_l , \quad (1)$$

where m is kite mass. Deduction of these forces can be found in [5], [11]. Considering turbulence $\mathbf{W_t}$ in any direction, the resulting wind is $\mathbf{W_l} := \mathbf{W_n} + \mathbf{W_t}$. The *kite* velocity is

$$\mathbf{W_a} := \begin{bmatrix} \dot{\theta}_a r_a & \dot{\phi}_a r_a \sin\theta_a & \dot{r}_a \end{bmatrix}_l^T , \quad (2)$$

and the *effective wind*, $\mathbf{W_e} := \mathbf{W_l} - \mathbf{W_a}$. The ratio between the difference in line length, Δl, and the airfoil wingspan, d, defines the kite *roll* angle, ψ, and the system input as $u := \sin\psi = \Delta l/d$. Electric power is obtained by unwinding the lines at a speed $\dot{r}_a$ from a drum connected to a generator on the ground.

Finally, the system dynamics are represented by the nonlinear model $\dot{\mathbf{x}} = f(\mathbf{x}, u, \mathbf{W_l})$ with the state vector

$$\mathbf{x} = \begin{bmatrix} \theta_a & \phi_a & r_a & \dot{\theta}_a & \dot{\phi}_a & \dot{r}_a \end{bmatrix}^T . \quad (3)$$

We note that this model assumes the kite body longitudinal axis to align itself instantaneously with $\mathbf{W_e}$. This alignment is a good approximation when $\mathbf{W_e} \approx \mathbf{W_a}$, which is a typical situation in the traction phase.

The numerical analysis presented henceforth regards a kite of mass $m = 300\,\text{kg}$, wingspan $d = 80\,\text{m}$, characteristic area $A = 500\,\text{m}^2$, and kept at a base angle of attack $\alpha_0 = 3.5°$, tethered by two lines of diameter $d_l = 4\,\text{cm}$ and density $\rho_l = 970\,\text{kg/m}^3$. This model has been validated with a small-scale prototype in [5], which the reader is referred to for further information on model and airfoil parameters such as the lift $C_l(\alpha)$ and drag $C_d(\alpha)$ coefficient curves.

A. Turning Angle Dynamics

During the traction phase we have $\|\mathbf{W_a}\| > 0$, which allows us to define the kite velocity *turning angle* ξ on the tangent plane $(\mathbf{e}_\theta, \mathbf{e}_\phi)_l$, as depicted in Fig. 2. Note that $\mathbf{W_a}$ is not contained in the plane if $\dot{r}_a \neq 0$, hence it is necessary to work with its projection $\mathbf{W_a^p} = \mathbf{W_a} - (\mathbf{W_a} \bullet \mathbf{e_r})\mathbf{e_r}$.

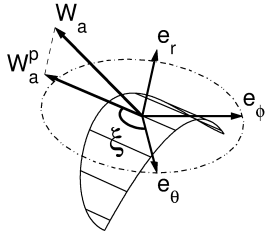

Fig. 2: Turning angle ξ and the tangent plane $(\mathbf{e}_\theta, \mathbf{e}_\phi)_l$.

As an alternative to the use of Liouville's theorem of differential geometry in [8], we define the turning angle as

$$\xi := \arccos(\mathbf{e}_\theta \bullet \mathbf{W}_\mathbf{a}^n)\,\text{sign}\left(-\arcsin(\mathbf{e}_\phi \bullet \mathbf{W}_\mathbf{a}^n)\right) + 2\pi\lambda , \quad (4)$$

where $\mathbf{W}_\mathbf{a}^n = \mathbf{W}_\mathbf{a}^p / \|\mathbf{W}_\mathbf{a}^p\|$ and λ is the number of accumulated rotations. Observe that ξ is a continuous, cumulative in multiple turns angle, as required in [8].

The time evolution of the turning angle depends on two factors. The first one refers to the gravity and is proportional to $\sin\xi$ to represent that this effect is maximum when the kite translates parallel to the ground and is zero when it points vertically. The second factor regards the control input. For a given input, the turning angle velocity is amplified or attenuated according to the effective wind.

Based on these physical considerations, we propose the nonlinear first-order model for the turning angle dynamics

$$\dot{\xi} := -K_g \sin\xi - K_\psi \|\mathbf{W_e}\| r_a^\kappa u , \quad (5)$$

where u is the control input. The effective wind $\mathbf{W_e}$ and the cable length r_a are supposed to be available online. A weak dependence of $\dot{\xi}$ with respect to r_a is represented by κ, which is typically a small coefficient. κ, K_g and K_ψ are constant parameters of the model, whose identification is discussed in the next section.

Observe in (5) that for $u = 0$ the system has a stable equilibrium at $\xi_{\text{eq}} = \pm 2k\pi$ and an unstable at $\xi_{\text{eq}} = \pi \pm 2k\pi$, $k \in \mathbb{N}$. Also, when $\xi \to \pm k\pi$, the kite points vertically and the system behaves approximately as an integrator.

It is important to emphasize that, as can be seen in (4), the turning angle is not well defined when $\|\mathbf{W_a}\| \to 0$. Another critical situation occurs near a stall condition. In this case, even if ξ could be defined, u loses ability to act on ξ, and therefore the model (5) is no longer valid.

B. Identification of the Turning Angle Model

Ten simulation experiments of 45 seconds each, with a 1000 Hz sampling rate, were carried out with the complete kite model borrowed from [5]. The following ranges of variables were considered: $\|\mathbf{W_n}\| \in [5, 25]\,\text{m/s}$, $r_a \in [300, 900]\,\text{m}$, $\theta_a \in [40, 85]°$, $|\phi_a| < 50°$, and $\|\mathbf{W_t}\| = 0$. From the experiments we calculated the parameters K_g and K_ψ by means of a nonlinear grey-box estimator using the Trust-Region Reflective Newton algorithm.

The first step in the identification procedure is to obtain κ. To that end, a preliminary identification was performed on model (5) with $\kappa = 0$. This was done by means of two experiments, corresponding to a bigger and smaller cable lengths ($\overline{r}_a$, $\underline{r}_a$) , rendering $\overline{K}_\psi$ and $\underline{K}_\psi$, respectively. We then compute κ as

$$\kappa = (\log\overline{K}_\psi - \log\underline{K}_\psi)/(\log\overline{r}_a - \log\underline{r}_a) , \quad (6)$$

resulting in $\kappa = 0.0526$. Next, we ran the ten mentioned experiments whose outcome is summarized in Table I.

The nominal parameter values were set as their average ones, $\breve{K}_g = 0.42440\,\text{rad/s}$ and $\breve{K}_\psi = 0.67895\,\text{rad/m}$, whereas the model identification quality was assessed by two

TABLE I
TURNING ANGLE IDENTIFICATION

		Min	Max	Std [%]	**Avg**
K_g	[rad/s]	0.33167	0.57206	19.4	**0.42440**
K_ψ	[rad/m]	0.65970	0.68490	1.3	**0.67895**

criteria: the *Akaike*'s Final Prediction Error (FPE) and the *model fit*, the latter being defined as

$$fit = 100\left(1 - \frac{\sqrt{\sum(y[k]-\hat{y}[k])^2}}{\sqrt{\sum(y[k]-\tilde{y}[k])^2}}\right), \quad (7)$$

where $y[k]$, $\hat{y}[k]$ and $\tilde{y}[k]$ are the sampled, predicted, and mean values of $\dot{\xi}$, respectively.

According to [12], the most accurate model has the smallest FPE and fit closest to 100. With $\breve{K}_g$ and $\breve{K}_\psi$ estimated above, it was achieved $fit > 93.03$ and $FPE < 0.0146$ (Table II) in all experiments. This indicates a good correlation between the proposed model (5) and the simulation experiments with the complete kite model from [5].

TABLE II
TURNING ANGLE MODEL VALIDATION

	Min	Max	**Avg**
FPE	0.00280	0.01460	**0.01007**
fit	93.03520	96.96890	**95.44467**

It is evident in Table I that the standard deviation of K_g is higher than that of K_ψ. However, it is not an issue since the model (5) has only a minor sensitivity to small variations of K_g. To illustrate this fact, the validation criteria of the model corresponding to the original ten experiments were recalculated considering four situations. In each situation, one parameter was disturbed 20% from its nominal value while keeping the other parameter as nominal. The average values of the FPE and fit criteria are shown in the Table III. Observe that, for a disturbed K_g, the validation criteria results remain similar to those of Table II.

TABLE III
EFFECT OF PARAMETER PERTURBATION ON THE VALIDATION CRITERIA

K_ψ / K_g	$\breve{K}_\psi$ / $0.8\breve{K}_g$	$\breve{K}_\psi$ / $1.2\breve{K}_g$	$0.8\breve{K}_\psi$ / $\breve{K}_g$	$1.2\breve{K}_\psi$ / $\breve{K}_g$
FPE	0.011	0.018	0.289	0.238
fit	94.49	93.96	78.51	79.87

III. CONTROL DESIGN

In order to achieve flight path reference tracking we propose a nonlinear control scheme with two loops (Fig. 3). The outer loop comprises the trajectory generator and provides a reference, ξ_{ref}, to the inner loop.

A. Inner Loop: Turning Angle Control

Assuming that $\mathbf{W_e}$, r_a and ξ are measured, we impose a linear dynamics to the turning angle error $e_\xi = \xi_{\text{ref}} - \xi$ as

$$\dot{e}_\xi = \dot{\xi}_{\text{ref}} - \dot{\xi} = -\gamma e_\xi \, . \quad (8)$$

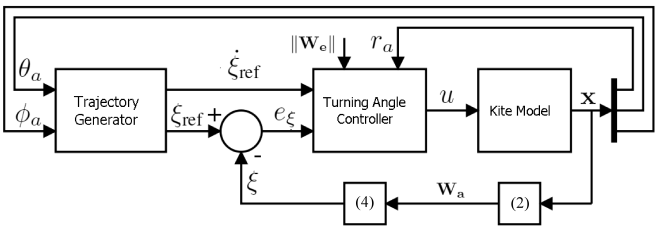

Fig. 3: Proposed control scheme.

Its speed of convergence is determined by the control parameter $\gamma > 0$. Recalling that $u = \sin\psi$, where ψ is the kite *roll* angle, by using the proposed model in (5) and *feedback linearization*, we arrive at the control law

$$u := -\frac{1}{K_\psi \|\mathbf{W_e}\| r_a^\kappa}\left[K_g \sin\xi + \dot{\xi}_{\text{ref}} + \gamma(\xi_{\text{ref}} - \xi)\right], \quad (9)$$

that ensures the asymptotic stability of $\dot{e}_\xi$ in (8) as long as no control saturation happens, i.e. $|u| < |\sin\overline{\psi}| \leq 1$ given a roll angle limitation $|\overline{\psi}| < \pi/2$. A study of the system stability with $u = \pm|\sin\overline{\psi}|$ remains to be done, even though saturation did not seem to be a problem, according to simulation results.

B. Outer Loop: Flight Trajectory Generation

It consists of a kinematic controller based on the lemniscate of Bernoulli (Fig. 4), a 2-dimensional geometric figure described in polar coordinates by the function

$$r_m = f(\omega) = a\sqrt{2\cos(2\omega)}\,, \quad (10)$$

where a is the focal length, and defined by the mapping

$$f(\omega) : \left[0, \frac{\pi}{4}\right] \cup \left(3\frac{\pi}{4}, 5\frac{\pi}{4}\right] \cup \left(7\frac{\pi}{4}, 2\pi\right) + 2k\pi \mapsto \mathbb{R}^+ \, , \quad (11)$$

$k \in \mathbb{N}$. The lemniscate has already been used for flight trajectory purposes, e.g. of UAVs [13]. We chose it given its resemblance with the optimal figure-eight trajectories in [3], [5], [7]. Moreover, smooth control action is expected since the lemniscate is a figure that is formed approximately from two semi-circles and two straight lines with a smooth transition between them. This is an interesting feature for reducing mechanical stress on the actuators.

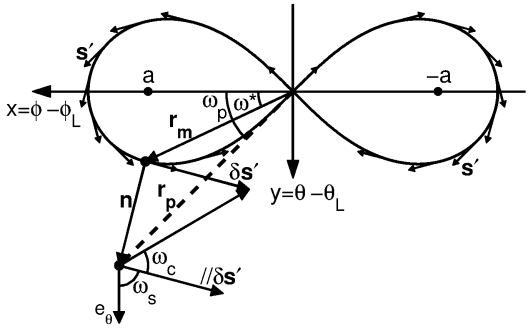

Fig. 4: Trajectory generation with Bernoulli's lemniscate.

Given the lemniscate center position $(\theta_L, \phi_L)_i$ in the spherical inertial frame, the kite position in the angular lemniscate frame is defined as the offset

$$\mathbf{r_p} = \begin{bmatrix} x_p & y_p \end{bmatrix}_L^T = \begin{bmatrix} \phi_a & \theta_a \end{bmatrix}_i^T - \begin{bmatrix} \phi_L & \theta_L \end{bmatrix}_i^T . \quad (12)$$

The distance between a general lemniscate point,

$$\mathbf{r_m} = \begin{bmatrix} x_m \\ y_m \end{bmatrix}_L = \begin{bmatrix} a\sqrt{2\cos(2\omega)}\cos\omega \\ a\sqrt{2\cos(2\omega)}\sin\omega \end{bmatrix}_L , \quad (13)$$

and the kite position is $\mathbf{n} = \mathbf{r_p} - \mathbf{r_m}$, whereas the tangent vector to the lemniscate trajectory is

$$\mathbf{s} = \frac{d\mathbf{r_m}}{d\omega} = \frac{a\sqrt{2}}{\sqrt{\cos(2\omega)}} \begin{bmatrix} -\sin(3\omega) \\ \cos(3\omega) \end{bmatrix}_L . \quad (14)$$

Note the existence of an inflection point at $\omega^\dagger = \pi/4 \pm k\pi/2$, $k \in \mathbb{N}$, where $\|\mathbf{s}(\omega^\dagger)\| \to \infty$ and $\mathbf{s}$ changes direction. To handle these issues and obtain a continuous derivative so that the kite always descends the lemniscate at its extremities, we shall work from now on with the normalized and direction-corrected $\mathbf{s}' = \text{sign}\big(\cos(\omega)\big)\mathbf{s}/\|\mathbf{s}\|$, i.e. we invert the direction of $\mathbf{s}$ in the semi-plane $x < 0$. The tangent vector angle ω_s is then calculated, similarly as the turning angle, by replacing $\mathbf{W_a^n}$ by $\mathbf{s}'$ in (4).

It is necessary to find $\omega^\star = \arg\min(\|\mathbf{n}(\omega)\|)$ in every control iteration in order to calculate the turning angle reference. We investigated two techniques employing numerical methods. The first one is by directly minimizing $\|\mathbf{n}(\omega)\|$ in the domain of the function (11) for a given k. The other one is by imposing the perpendicularity condition $\mathbf{n} \bullet \mathbf{s}' = 0$ and finding the root of the resulting equation

$$y_p\cos(3\omega) - x_p\sin(3\omega) + a\sqrt{2\cos(2\omega)}\sin(2\omega) = 0 . \quad (15)$$

Observe that (15) has four possible solutions for a given k in the domain of (11). Therefore, to ensure that the solution found corresponds to $\omega^\star$, we restrict the root-searching method to a small enough sliding ω-window centered in the solution obtained in the previous iteration.

We define the magnitude of the *correction angle* ω_c as

$$|\omega_c| := \arctan(\|\mathbf{n}(\omega^\star)\|/\delta) , \quad (16)$$

where $\delta > 0$ is a control parameter. One can think of δ as the distance parallel to $\mathbf{s}'$ that the kite would have to travel for achieving $\|\mathbf{n}\| = 0$ if $\mathbf{s}$ would not change direction. In order to accomplish a trajectory correction of the kite towards the lemniscate at the nearest point $\mathbf{r_m}(\omega^\star)$, we take the cross product of the orthogonal vectors $\mathbf{s}'$ and $\mathbf{n}(\omega^\star)$

$$\mathbf{q} = \begin{bmatrix} q_x & q_y & q_z \end{bmatrix}^T = \mathbf{s}' \times \mathbf{n}(\omega^\star) , \quad (17)$$

and designate a sign to (16) as $-\text{sign}(q_z)$, allowing us to define the turning angle reference as

$$\xi_{\text{ref}} := \omega_s + \omega_c = \omega_s - \text{sign}(q_z)|\omega_c| . \quad (18)$$

C. Control Tuning

According to (8), any $\gamma = 1/\tau > 0$ ensures asymptotic stability of e_ξ (inner loop), where τ is its desired time constant. Nevertheless, high values of γ cause control action saturation, whereas low values of γ result in a high e_ξ. If this tracking error gets high enough, the kite might collide with the ground. Therefore we need to ensure that e_ξ converges significantly faster than an orbit period, known *a priori* to be around 6 s. By dividing an orbit into 30 segments, and requiring e_ξ to converge inside each segment duration, we get $4\tau = 4/\gamma = 6/30$, i.e. $\gamma = 20$.

For the outer-loop, the same compromise between (position) reference tracking error and control saturation applies. As in this example we have $a\, r_a = 64\,\text{m}$, a satisfactory choice was found to be $\delta = 8$.

IV. OPTIMIZATION

An offline optimization is necessary for establishing the conditions in which the system should be operated to achieve maximal wind power extraction. Note that here we will optimize the operation point

$$\nu = \begin{bmatrix} \theta_L & \phi_L & r_a & \dot{r}_a & a \end{bmatrix} \quad (19)$$

considering only the traction phase, whereas in [3], [5] also the passive phase was considered, influencing the optimization outcome ν^*.

As shown in [5], [7], the instantaneous electric power generated by the system can be approximated by

$$P = F_{\text{trac}}\dot{r}_a\eta = C(\alpha)\|\mathbf{W_{e,r}}\|^2\,\dot{r}_a\eta , \quad (20)$$

where $C(\alpha)$ is a coefficient used to estimate the traction force F_{trac} equally divided between the cables, η is an assumed efficiency in converting mechanical to electric power, and

$$\|\mathbf{W_{e,r}}\| = |W_x(r_a\cos\theta_a)\sin\theta_a\cos\phi_a - \dot{r}_a| \quad (21)$$

is the component of the effective wind vector on the $\mathbf{e_r}$ direction. $W_x(z_a)$ is the nominal wind speed along $\mathbf{x_i}$ at height z_a according to the logarithmic wind model for the site of Brindisi in Italy during winter, as used in [5].

All components of the operation point (19), expect for a, can be optimally found by maximizing (20) considering their average values in one lemniscate orbit, and that $\tilde{\theta}_a = \theta_L$ and $\tilde{\phi}_a = \phi_L$, yielding an average orbit net power $\tilde{P}$.

Fig. 5 illustrates the effect of a on F_{trac}, where the system was simulated with $(r_a, \dot{r}_a) = (300\,\text{m}, 0\,\text{m/s})$ and step-variations expressed by the vector $\theta_\mathbf{L} = (45, 60, 75)^\circ$. For each step on θ_L, a was also step-varied as $\mathbf{a} = (5, 10, 20)^\circ$.

A decrease on a renders a higher $\tilde{F}_{\text{trac}}$ and usually a smaller $\sigma(F_{\text{trac}})$ – both desired effects depicted in Fig 5 – however it causes $|\psi|$ and $|\dot{\psi}|$ to increase. Therefore a lower bound on a can be obtained from the control limitations as $\underline{a}(|\overline{\psi}|, |\overline{\dot{\psi}}|)$. Another constraint for maximizing (20) regard a minimal flight elevation, that translates into $\overline{\theta}_L$, to ensure a minimal distance $\underline{z}_a$ between the kite and the ground.

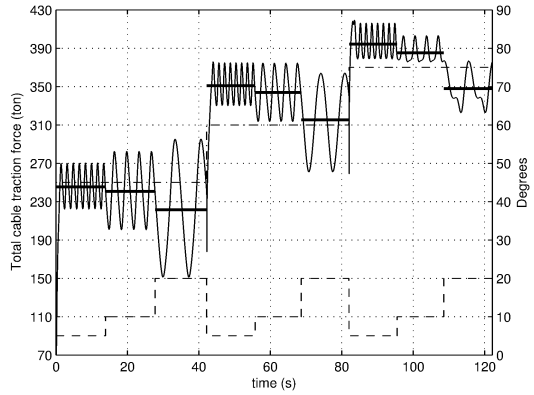

Fig. 5: Dependence of F_{trac} (—) and $\tilde{F}_{\text{trac}}$ (**—**) on θ_L (– ·) and a (– –).

Also, a maximal unwinding speed of the cables, $\overline{\dot{r}}_a$, and a maximal cable traction force, $\overline{F}_{\text{trac}}$, are considered. Due to space limitations, deduction of these constraints were omitted. Thus, the optimization problem can be stated as

$$\nu^* = (\theta_L^*, \phi_L^*, r_a^*, \dot{r}_a^*) = \arg\max \tilde{P}\,(\theta_L, \phi_L, r_a, \dot{r}_a) \quad (22)$$

such that the argument constraints are satisfied, and given W_x, Δr_a and α.

We highlight that the optimization outcome is influenced by the choice of the attack angle. Therefore, given an initial guess $\nu^\diamond$ of the optimal operation point, we run (22) with $\alpha(\nu^\diamond)$. We can fine-tune ν^* at the beginning of each traction phase by re-running (22) with the previous α^*.

V. SIMULATION RESULTS

With $(\alpha^\diamond, \Delta r, \underline{z}_a) = (7.8°, 100\,\text{m}, 80\,\text{m})$ and control limitations $(|\overline{\psi}|, |\overline{\dot{\psi}}|) = (6°, 3°/\text{s})$ we obtained $a^* r_a = 64.3\,\text{m}$ and $\nu^* = (79.7°, 0°, 652\,\text{m}, 2.71\,\text{m/s})$ with a theoretical optimal power $\tilde{P}^*_{\text{thr}} = 3551\,\text{kW}$ for an efficiency $\eta = 0.8$. By simulation the net power obtained was $\tilde{P}^*_{\text{sim}} = 3468\,\text{kW}$, i.e. a 2.3% estimation error from $\tilde{P}^*_{\text{thr}}$ and approximately 16% higher than that of the optimized system, with same parameters, presented in [5] for the traction phase. Moreover, $\tilde{P}^*_{\text{sim}}$ corresponded approximately to the average for the whole interval Δr_a, which we will refer to as the nominal power $P_{\text{nom}} = 3474\,\text{kW}$.

The net power behaviour in a broader span than $r_a^* \pm \Delta r_a/2$ is illustrated in Fig. 6. Observe that higher $\tilde{P}_{\text{sim}}$ values are achieved for $r_a < \underline{r}_a$, nevertheless possibly violating the constraints $\overline{F}_{\text{max}}$ and $\underline{z}_a$. On the other hand, mean and minimal orbit power tend to diminish for $r_a > \overline{r}_a$, whereas the maximal power decreases less rapidly, thus increasing the standard deviation of P_{sim}, which is generally undesired. Similar curves apply to F_{trac}, $\|\mathbf{W_a}\|$ and $\|\mathbf{W_e}\|$.

It took $6\,\text{s}$ to complete a lemniscate orbit with ν^*, quite short in comparison to the $20\,\text{s}$ of the closed orbit in [4] since, for power maximization, open and closed orbit approaches have opposite criteria regarding orbit perimeter and consequently period. Kite flight altitude in Δr_a was kept inside $80\,\text{m} \le z_a \le 156\,\text{m}$ while α slowly increased with r_a

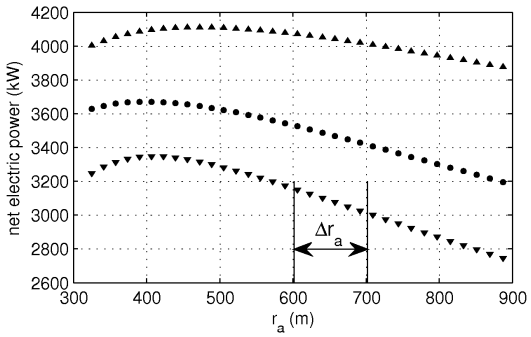

Fig. 6: Courses of mean (•) and peak values of $P_{\text{sim}}(r_a)$ with ν^*.

at an approximately constant rate of $0.0052°/\text{s}$. The peak on the total traction force was 7% below the safety limit of the cable. Table IV summarizes some simulation values.

TABLE IV
NOMINAL SIMULATION RESULTS WITH ν^*

		mean	max	min	std [%]
P_{sim}	[kW]	3474	4072	3024	9.7
F_{trac}	[ton]	163.2	191.4	142	9.7
α	[deg]	7.63	8.08	7.13	3.7
$\|\mathbf{W_a}\|$	[km/h]	269	303	243	7.2
$\|\mathbf{W_e}\|$	[km/h]	270	297	248	5.8

It was observed that r_a^* obtained with (22), and consequently $\tilde{P}^*_{\text{thr}}$, varied significantly with the initial guess fed to the optimizer due to local maxima, as pointed out in [3].

A. Control Performance

The resulting control action can be seen in Fig. 7 as the thin curve, whereas the thick one illustrates how the shape of ψ changes with the increase of the product $a\,r_a$, becoming quite similar to the one in [8]. Both curves were obtained with $r_a \in (652 \pm 50)\,\text{m}$ and $\dot{r}_a = 2.71\,\text{m/s}$. We can see that, for $a\,r_a$ large enough, as the kite approaches the lemniscate origin ψ tends to a constant value different from zero in order to compensate for the gravity influence represented by $-K_g \sin\xi$ in (5).

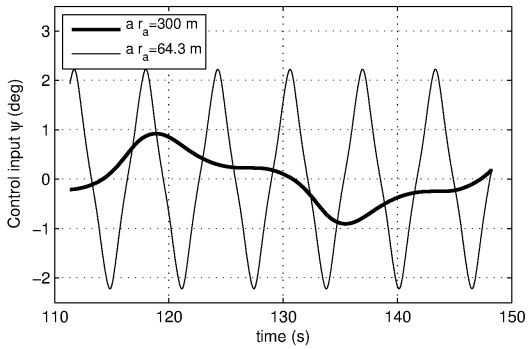

Fig. 7: Control action for optimized (—) and increased (**—**) $a\,r_a$.

Control constraints were also fully respected, with the maximum values obtained by simulation $|\overline{\psi}|_{\text{sim}} \approx 2.2° < |\overline{\psi}|$ and $|\overline{\dot{\psi}}|_{\text{sim}} \approx 2°/\text{s} < |\overline{\dot{\psi}}|$. Moreover, their peaks are constant and dependent essentially on $a\,r_a$. Note that $|\overline{\dot{\psi}}|$ is especially

important, since e.g. $3^\circ/\text{s}$ means the actuator being able to reel in or out approximately 4 m/s of cable, which is within our allowable speed limit of $\overline{\dot{r}}_a = 6\,\text{m/s}$, whereas the constraint of $20^\circ/\text{s}$ used in [5] requires around 27 m/s of reel speed, i.e. about 4 times greater than $\overline{\dot{r}}_a$.

In terms of reference tracking our controller yielded a slight turning angle error with $\tilde{e}_\xi \approx 0^\circ$, $\sigma(e_\xi) = 1.29^\circ$ and $|\overline{e}_\xi| = 2.16^\circ$, whereas the position error, defined as

$$\mathbf{e_p} := \begin{bmatrix} r_a\big(\sin(\theta_L + y_m)\cos x_m - \sin\theta_a \cos\phi_a\big) \\ r_a\big(\sin(\theta_L + y_m)\sin x_m - \sin\theta_a \sin\phi_a\big) \\ r_a\big(\cos(\theta_L + y_m) - \cos\theta_a\big) \end{bmatrix}_i , \quad (23)$$

was characterized by $\|\tilde{\mathbf{e}}_\mathbf{p}\| = 0.18\,\text{m}$, $\sigma(\|\mathbf{e_p}\|) = 0.09\,\text{m}$ and $\|\overline{\mathbf{e}}_\mathbf{p}\| = 0.34\,\text{m}$, i.e. approximately 3.5 times less than the mean linear tracking error of about 0.65 m with no wind disturbance claimed in [8].

B. Turbulent Wind

In order to analyse our control performance under turbulent wind conditions, we used the *Dryden* model following Military Specification MIL-F-8785C [14]. In short, it reproduces turbulent wind by passing band-limited white noise through shaping filters. Turbulence intensity $\zeta(z_a)$ for $z_a < 304.8\,\text{m}$ (1000 ft) is given in the lateral (la), longitudinal (lo) and vertical (ve) directions as

$$\begin{aligned} \zeta_{\text{ve}} &= 0.1 W_{\text{ref}} = W_x(z_a)/k \\ \zeta_{\text{la}} = \zeta_{\text{lo}} &= \frac{1}{(0.177 + 0.0027\,z_a)^{0.4}}\zeta_{\text{ve}} \end{aligned} \quad (24)$$

where W_{ref} is a reference wind speed. For our analysis we chose $z_a = 115\,\text{m}$ and decreased k starting from 40, i.e. we progressively increased ζ with respect to $W_x(z_a)$ until the kite stalled. Simulations results are here suppressed due to space restrictions. It was observed that, as long as the control was able to maintain the kite flying despite turbulence, both e_ξ and $\|\mathbf{e_p}\|$ remained quite constant at low levels. This seems to be agree with [8] for a correlation rate of 1.

Although in terms of reference tracking our controller coped well with wind turbulence, power generation was severely affected, as can be seen in Fig. 8. With $k = 10 \Rightarrow \zeta_{\text{la}} = 1.1\,\text{m/s}$, the instantaneous power output oscillated much more than in the nominal case, yielding $\sigma(P_{\text{sim}}) = 26.6\,\%$ and reaching peaks up to $\overline{P}_{\text{sim}} = 7849\,\text{kW}$, i.e. 126 % bigger than P_{nom}. Recalling that a machine has to be sized for its peak power, the impact of wind turbulence on P_{sim} needs to be addressed, possibly by manipulating $\dot{r}_a$ and α_0.

VI. FINAL REMARKS

In this paper we proposed an alternative model for the turning angle dynamics of a power kite and the identification of the model parameters was discussed. The control law was obtained through feedback linearization in order to track an offline optimized trajectory based on Bernoulli's lemniscate. Our simulation values of power generation in the traction phase were 16% higher than those in [5]. Also, a better trajectory tracking performance was obtained with the mean

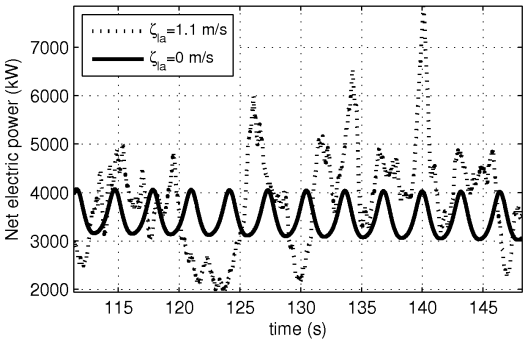

Fig. 8: Net power output affected by wind turbulence.

position error about 3.5 times smaller than in [8]. Error values were kept small even under turbulent wind, provided the turbulence did not cause the kite to stall.

In order to accomplish a full operation cycle for the pumping kite, a control strategy for the passive phase remains to be developed. Also, a measuring system of $\|\mathbf{W_e}\|$ has to be investigated, since our feedback linearization controller relies on that measurement. Finally, a power control loop needs to be conceived to cope with wind turbulence, thus allowing the system to operate in harsher wind conditions.

REFERENCES

[1] International Energy Agency (IEA), "World energy outlook 2012," 2012, ISBN 978-92-64-18084-0.

[2] M. Ahmed, A. Hably, and S. Bacha, "High altitude wind power systems: A survey on flexible power kites," in *XXth International Conference on Electrical Machines*, Marseille, France, September 2012.

[3] B. Houska and M. Diehl, "Optimal control for power generating kites," in *European Control Conference*, Kos, Greece, July 2007, pp. 1–14.

[4] P. Williams, B. Lansdorp, and W. Ockels, "Nonlinear control and estimation of a tethered kite in changing wind conditions," *Journal of Guidance, Control, and Dynamics*, vol. 31, no. 3, pp. 793–798, May-June 2008.

[5] L. Fagiano, "Control of tethered airfoils for high-altitude wind energy generation," Ph.D. dissertation, Politecnico di Torino, Torino, Italy, 2009.

[6] M. Ahmed, A. Hably, and S. Bacha, "Power maximization of a closed-orbit kite generator system," in *50th IEEE Conference on Decision and Control and European Control Conference*, Orlando, FL, USA, December 2011, pp. 7717–7722.

[7] I. Argatov and R. Silvennoinen, "Energy conversion efficiency of the pumping kite wind generator," *Renewable Energy*, vol. 35, pp. 1052–1060, 2010.

[8] J. H. Baayen and W. Ockels, "Tracking control with adaption of kites," *IET Control Theory & Applications*, vol. 6, no. 2, pp. 182–191, January 2012.

[9] J. H. Baayen, "Automatic trajectory tracking control of kites," Master's thesis, Delft University of Technology, Delft, the Netherlands, March 2011.

[10] M. Erhard and H. Strauch, "Control of towing kites for seagoing vessels," *IEEE Transactions on Control Systems Technology*, vol. 21, no. 5, pp. 1629–1640, November 2012.

[11] M. M. Diehl, "Real-time optimization for large scale nonlinear processes," Ph.D. dissertation, Ruprecht-Karls-Universität, Heidelberg, Germany, 2001.

[12] L. Ljung, *System Identification: Theory for the User*, 2nd ed. Englewood Cliffs, NJ, USA: Prentice Hall, 1999.

[13] A. C. Vaughn, "Path planning and control of unmanned aerial vehicles in the presence of wind," Master's thesis, University of California, Berkeley, CA, USA, 2003.

[14] M. V. Cook, *Flight Dynamics Principles: A Linear Systems Approach to Aircraft Stability*, 3rd ed. Waltham, MA, USA: Butterworth-Heinemann, 2013.